Supporting Information

Structure-Relaxivity Mechanism of Ultrasmall Ferrite Nanoparticle T_1 MR Contrast Agent: The Impact of Dopants Controlled Crystalline Core and Surface Disordered Shell

*Yuqing Miao,[a, 1] Huan Zhang,[a, 1] Jing Cai,[b] Yimin Chen,[a] Huijun Ma,[c] Shuo Zhang,[d] Jia Bao Yi,[e] Xiaoli Liu,[f] Boon-Huat Bay,[g] Yingkun Guo,[h] Xin Zhou,[i] Ning Gu,[j] and Haiming Fan,[a,]**

[a] Key Laboratory of Synthetic and Natural Functional Molecule Chemistry of the Ministry of Education, College of Chemistry and Materials Science, Northwest University, Xi'an, 710069, China.

[b] State Key Laboratory of Oncology in South China, Sun Yat-sen University Cancer Center, Collaborative Innovation Center for Cancer Medicine, Guangzhou, 510060, China.

[c] National Demonstration Center for Experimental Chemistry Education, College of Chemistry and Materials Science, Northwest University, Xi'an, 710069, China.

[d] Shanghai Institute of Applied Physics, Chinese Academy of Sciences, Shanghai, 201204, China.

[e] Global Innovative Centre for Advanced Nanomaterials, School of Engineering, The University of Newcastle, Callaghan, New South Wales 2308, Australia.

[f] Key Laboratory of Resource Biology and Biotechnology in Western China, Ministry of Education. School of Medicine, Northwest University, Xi'an, 710069, China.

[g] Department of Anatomy, Yong Loo Lin School of Medicine, National University of Singapore, 4 Medical Drive, MD10, 117594, Singapore.

[h] Sichuan University, West China University Hospital 2, Key Lab Birth Defects & Related Dis Women & Child of the Ministry of Education, Department of Radiology, 20 Sect 3 South Renmin Road, Chengdu 610041, Sichuan, China.

[i] State Key Laboratory of Magnetic Resonance and Atomic and Molecular Physics, National Center for Magnetic Resonance in Wuhan, Wuhan Institute of Physics and Mathematics, Chinese Academy of Sciences, Wuhan, 430071, China.

[j] State Key Laboratory of Bioelectronics, Jiangsu Key Laboratory for Biomaterials and Devices, School of Biological Science and Medical Engineering, Southeast University, Nanjing 210096, China.

[1] These authors contributed equally.

* Corresponding Author: Haiming Fan

E-mail: fanhm@nwu.edu.cn

1. Experimental section

Materials

Ferric chloride hexahydrate (>99%) gadolinium nitrate hexahydrate (>99%) and Copper chloride dihydrate (>99%) were purchased from Sinopharm Chemical Reagent Co., Ltd. Erucic acid was procured from Shanghai Aladdin Co., Ltd. Zinc hydroxide carbonate (>99%) and manganese chloride tetrahydrate (>99.0%) were obtained from Fuchen Chemical Technology Co., Ltd. Benzyl ether and 3, 4-dihydroxyhydrocinnamic acid (DHCA) were purchased from Sigma-Aldrich Co., Ltd. Oleyl alcohol (65.0%) was purchased from TCI Co., Ltd. All the reagents were used without any further purification.

Characterizations

Transmission electron microscope (TEM) and high-resolution TEM (HRTEM) measurements were conducted using a transmission electron microscope (FEI, Talos F200x). X-ray diffraction patterns were recorded on a Bruker D8 Advanced Diffractometer using Cu/Kα radiation (λ = 1.5418 Å). Magnetic characterizations of the samples were performed using a superconducting quantum interference device (SQUID) magnetometer (MPMS-XL-7). The hydrodynamic diameters of the samples were evaluated with dynamic light scattering (DLS, Malvern Zetasizer nano-ZS instrument). Elemental analysis was performed using inductively coupled plasma atomic emission spectroscopy (ICP-AES). X-ray absorption fine structure (XAFS) spectra of Fe, Mn, and Zn K-edge were collected at room temperature in transmission mode at the beamline BL14W1 of Shanghai Synchrotron Radiation Facility (SSRF).

Synthesis of $Zn_xF@Zn_xMn_yF$ nanoparticles

The 3.8 nm ultrasmall Zn_xF nanoparticles were first prepared based on the previously reported dynamic simultaneous thermal decomposition (DSTD) method.[1] In a typical synthesis of $Zn_{0.4}F$ nanoparticles, iron-eruciate complex (2.14 g), zinc hydroxide carbonate (0.09 g), oleyl alcohol (3.22 g), and benzyl ether (10 g) were mixed in a 50 ml three-necked, round-bottomed flask. The mixed solution was heated to 260 °C and it was maintained for another 30 min in the presence of an argon atmosphere. The heat source was then removed, and the reaction mixture was cooled down quickly to room temperature. Upon the addition of ethanol, a black precipitate was isolated by centrifugation. The obtained $Zn_{0.4}F$ nanoparticles were then dissolved in hexane for further use. To adjust the Zn doping level (x) in the sample, various amounts of iron-eruciate complex and zinc hydroxide carbonate were used. A summary of the detailed reaction parameters is shown in Table S1. The cation exchange reaction was then carried out for the obtained $Zn_xF@Zn_xMn_yF$ nanoparticles. In a typical setup, 1 mL of $Zn_{0.4}F$ nanoparticles (500 mM) and 1 mL of $MnCl_2{\cdot}4H_2O$ (10-35 mM) were dispersed in 5 ml of tetrahydrofuran (THF). The mixture was heated to 60 °C, and it was maintained for 30 min under magnetic stirring. After cooling down to room temperature, the mixture was purified *via* centrifugation. $Zn_xF@Zn_xGd_yF$ and $Zn_xF@Zn_xCu_yF$ nanoparticles were obtained *via* the same procedure, with $Gd(NO)_3{\cdot}6H_2O$ and $CuCl_2{\cdot}2H_2O$ used as precursors, respectively.

Surface modification of Zn_xF nanoparticles with DHCA

The surface modification was performed using a ligand-exchange reaction.[2] Briefly, 50 mg of DHCA and 20 mg of the as-prepared UFNPs were mixed with the addition of 10 mL of THF. The resulting solution was heated to 50 °C for the surface ligand exchange reaction to take place. After a 3 hours reaction, the mixture was cooled down to room temperature, and 500 μL NaOH (0.5 M) was added to precipitate the nanoparticles. The sediment was collected *via* centrifugation, and it was re-dispersed in water for further use.

Synthesis of $Zn_{0.4}F@Zn_{0.4}Mn_{0.2}F$-AMD

To conjugate the as-prepared sample with AMD3100, 10 μL of 1-ethyl-3-(3-dimethylaminopropyl) carbodiimide hydrochloride (EDC) (50 mM) was added into 5 mL $Zn_{0.4}F@Zn_{0.4}Mn_{0.2}F$ solution (5 mM). The mixture was incubated for 15 min with shaking. Then, 10 μL of N-hydroxysuccinimide (NHS) (25 mM) and AMD3100 (2 μmol) were added and co-incubated for 4 hours. Finally, the $Zn_{0.4}F@Zn_{0.4}Mn_{0.2}F$-AMD nanoparticles were collected *via* centrifugal ultrafiltration (MWCO 5 kDa).

MR relaxivity measurements

In vitro MR relaxivities of the UFNPs were tested by a clinical MRI scanner system (3.0 T, Siemens, Germany). T_1-weighted images were acquired using an echo time (TE) 19 ms, a repetition time (TR) 4000 ms and the parameter to obtain T_2-weighted images were as follows: TR = 5000 ms and TE = 13-320 ms.

in vivo MRI:

The *in vivo* MR images were acquired on a 7.0 T 70/20 Bruker BioSpec small animal MRI system. To establish the subcutaneous breast tumor model, 5×10^6 cells 4T1 cells were subcutaneously injected into left back of the mice (n = 3). When the tumor size

reached around 80 mm^3, the mice were anesthetized and then the nanoprobe (5 mg [Zn+Mn+Fe]/kg body weight) was injected through the tail vein. T_1-weighted images were acquired at designated time intervals. The scanning parameters for T_1 imaging were set as follows: FOV= 35 × 35 mm^2, TR= 300 ms, TE = 5.0 ms, flip angle = 90° and NEX = 8.

To establish the breast cancer lung metastasis model, 2 × 10^5 4T1-Luc breast cells in 150 μL PBS were injected intravenously into BALB/C mice. The mice were randomly assigned to two groups (2 and 5 days, n = 3). All mice were imaged with MRI and BLI (PerkinElmer, USA) to detect metastases in the lung. T_1-weighted images were acquired at designated time intervals. The scanning parameters for T_1 imaging were set as follows: FOV= 30 × 30 mm^2, TR= 300 ms, TE = 5.0 ms, flip angle = 90° and NEX = 8. After imaging, the mice were sacrificed and the lung tissues in each group were collected for H&E staining. All animal experiments were carried out under a protocol approved by the Institutional Animal Care and Use Committee of Northwest University.

Cellular cytotoxicity

The CCK-8 assay was performed to test the *in vitro* cytotoxicity of $Zn_{0.4}F@Zn_{0.4}Mn_{0.2}F$-AMD. Briefly, MCF-7 cells or 4T1 cells were seeded in a 96-well plate at a density of 10^4 cells $well^{-1}$. After 24 h incubation for the cell attachment, 0.1 mL $Zn_{0.4}F@Zn_{0.4}Mn_{0.2}F$-AMD of different concentrations (0-150 μg/mL) was added into the 96-well plate, and then the cells were tested with a CCK-8 assay after 24 h incubation. The absorbance value at 450 nm was determined by a microplate reader.

Pharmacokinetic study

The Balb/c mice (Female, 6–8 weeks, n = 3 for each nanoprobe) were intravenously injected with $Zn_{0.4}F@Zn_{0.4}Mn_{0.2}F$-AMD (5 mg/kg body weight), followed by the collection of ~100 μL blood samples from retro-orbital at 2, 5, 10, 30 min, 1, 3, 5, 8,

12, and 24 h p.i. The blood samples were completely digested by aqua regia overnight at room temperature. Subsequently, the solution was then diluted to 10 mL using deionized water. After which, the samples passed through a 0.45-μm filter to remove the insoluble components. The final samples were analyzed with ICP-MS.

Biodistribution

BALB/c mice (Female, 6–8 weeks) were intravenously injected with $Zn_{0.4}F@Zn_{0.4}Mn_{0.2}F$-AMD (5 mg/kg body weight), and they were sacrificed after 24 h. Then, the major organs (heart, liver, spleen, lung, kidney, and brain) were collected and measured by ICP-MS to detect the metal concentration.

Excretion of the $Zn_{0.4}F@Zn_{0.4}Mn_{0.2}F$-AMD

To test the excretion of $Zn_{0.4}F@Zn_{0.4}Mn_{0.2}F$-AMD, BALB/c mice (Female, 6–8 weeks, n = 3) were intravenously injected with $Zn_{0.4}F@Zn_{0.4}Mn_{0.2}F$-AMD (5 mg/kg body weight). Mouse urine and feces were collected at 5 h, 8 h, 12 h, 24 h, 48 h, and 72 h post-injection. The amount of metal in the urine and feces were determined using ICP-MS.

Statistics:

Statistical analysis was carried out using GraphPad Prism 5 software. The data number for each group was≥3, and the results were expressed as Mean ± SD. Asterisks denote statistical significance: *$p < 0.05$, **$p < 0.01$, ***$p < 0.001$.

2. Theoretical Simulations

With regards to the T_1 contrast agents, the T_1 relaxivity can be derived by summing the contributions of the inner-sphere r^{IS} and outer-sphere r^{OS} relaxivities, in accordance with the classical Solomon–Bloembergen–Morgan (SBM) theory,[3-4]

$$\frac{1}{T_1} = \left(\frac{1}{T_1}\right)_{inner\ sphere} + \left(\frac{1}{T_1}\right)_{outer\ sphere} \quad (1)$$

The inner-sphere contribution r^{IS} is given as;

$$\left(\frac{1}{T_1}\right)_{inner\ sphere} = \frac{qP_M}{T_{1M} + \tau_M} \quad (2)$$

where, q is the number of water molecules bound to the metal ion; P_M is the mole fraction of the metal ions; T_{1m} denotes the relaxation time of water molecules, and τ_m is the residence lifetime of the bound water.

T_{1m} can be expressed as;

$$\frac{1}{T_{1m}} = \frac{2}{15}\frac{\gamma_I^2 g^2 S(S+1)\beta^2}{r^6}\left[\frac{7\tau_{c2}}{1+\omega_s^2\tau_{c2}^2} + \frac{3\tau_{c1}}{1+\omega_I^2\tau_{c1}^2}\right] + \frac{2}{3}S(S+1)\left(\frac{A}{\hbar}\right)^2\left[\frac{\tau_{e2}}{1+\omega_s^2\tau_{e2}^2}\right] \quad (3)$$

where, γ_I is stated as the proton gyromagnetic ratio, g is the electronic g-factor, S is the total electron spin of the metal ion, β is the Bohr magneton, r is the distance of proton-metal ion, A/ħ is the electron-nuclear hyperfine coupling constant, ω_s and ω_I are the electronic and proton Larmor precession frequencies, respectively.

The correlation times τ_c and τ_e are defined as;

$$\frac{1}{\tau_{ci}} = \frac{1}{T_{ie}} + \frac{1}{\tau_m} + \frac{1}{\tau_R} \qquad i = 1, 2 \quad (4)$$

$$\frac{1}{\tau_{ei}} = \frac{1}{T_{ie}} + \frac{1}{\tau_m} \qquad i = 1, 2 \quad (5)$$

T_{1e} is the longitudinal electron spin relaxation time, and τ_R is the rotational tumbling time. The T_{ie} is defined as;

$$\frac{1}{T_{1e}} = \frac{1}{25}\Delta^2\tau_v[4S(S+1) - 3]\left[\frac{1}{1+\omega_s^2\tau_v^2} + \frac{4}{1+4\omega_s^2\tau_v^2}\right] \quad (6)$$

$$\frac{1}{T_{2e}} = \frac{1}{50}\Delta^2\tau_v[4S(S+1)-3]\left[\frac{5}{1+\omega_s^2\tau_v^2}+\frac{2}{1+4\omega_s^2\tau_v^2}+3\right] \quad (7)$$

where, Δ^2 is the mean square zero-field splitting (ZFS) energy, and τ_v is the correlation time for splitting.

The out-sphere contribution to the longitudinal relaxivity r^{OS} is given as[5]

$$\left(\frac{1}{T_1}\right)_{out\ sphere} = \frac{128\pi^2\gamma_I^2 M_n}{405\rho}\left(\frac{1}{1+L/a}\right)^3 M_S^2\tau_D J_A(\sqrt{2\omega_I\tau_D}) \quad (8)$$

where, Ms is the saturation magnetization of the nanoparticles, L is the thickness of surface impermeable molecule layer, a is the radius of the nanoparticles, τ_D is the translational diffusion time.

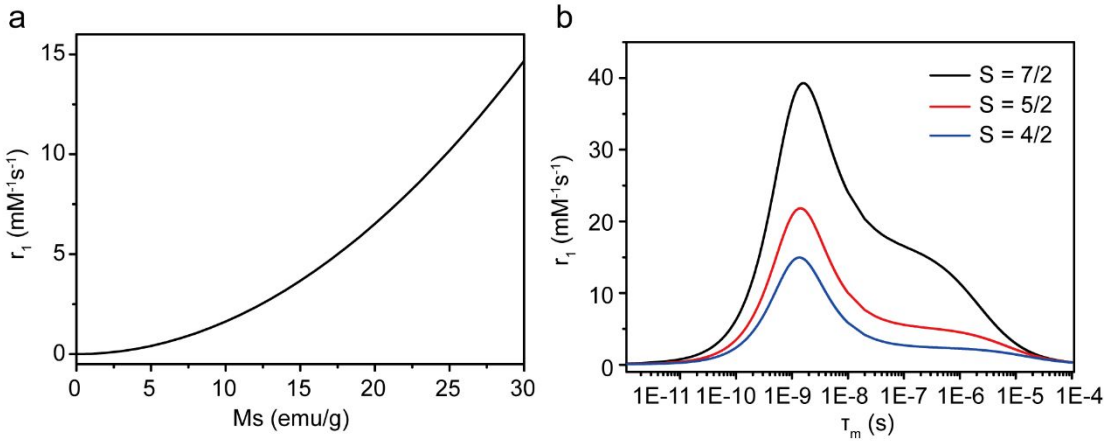

Figure S1. Simulated r_1 relaxivities of 3 nm UFNPs as a function of magnetization moment of crystalline core and the residence lifetime of the bound water (τ_m) of surface substituted atom using outer-sphere and inner-sphere models, respectively.

Table S1. Detailed reaction parameters for the synthesis of ultrasmall Zn_xF nanoparticles

Samples	Fe-eruciate (g)	Zinc hydroxide carbonate (g)	Oleyl alcohol (g)	Benzyl ether (g)	Heating rate (℃/min)	Aging temperature (℃)
$Zn_{0.2}F$	2.14	0.01	3.22	10	5	260
$Zn_{0.2}F$	2.14	0.03	3.22	10	5	260
$Zn_{0.3}F$	2.14	0.06	3.22	10	5	260
$Zn_{0.4}F$	2.14	0.09	3.22	10	5	260
$Zn_{0.5}F$	2.14	0.12	3.22	10	5	260
$Zn_{0.6}F$	2.14	0.15	3.22	10	5	260
$Zn_{0.7}F$	2.14	0.18	3.22	10	5	260
$Zn_{0.8}F$	2.14	0.24	3.22	10	5	260
$Zn_{0.9}F$	2.14	0.3	3.22	10	5	260

Table S2. Detailed reaction parameters for the synthesis of γ-Fe_2O_3@Mn_yF nanoparticles

Samples	$C_{\gamma\text{-}Fe2O3}$ (mM)	C_{MnCl2} (mM)	THF (mL)	Temperature (℃)	Time (min)
γ-Fe_2O_3@$Mn_{0.26}F$	500	10	5	60	30
γ-Fe_2O_3@$Mn_{0.28}F$	500	15	5	60	30
γ-Fe_2O_3@$Mn_{0.31}F$	500	20	5	60	30
γ-Fe_2O_3@$Mn_{0.35}F$	500	25	5	60	30
γ-Fe_2O_3@$Mn_{0.42}F$	500	30	5	60	30
γ-Fe_2O_3@$Mn_{0.43}F$	500	35	5	60	30

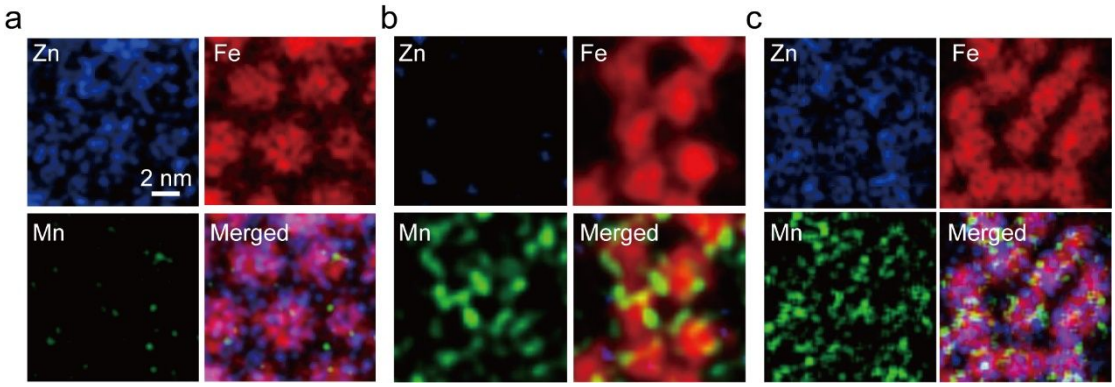

Figure S2. EDS mappings of $Zn_{0.4}F$ (a), γ-Fe_2O_3@$Mn_{0.4}F$ (b), and $Zn_{0.4}F$@$Zn_{0.4}Mn_{0.2}F$ (c).

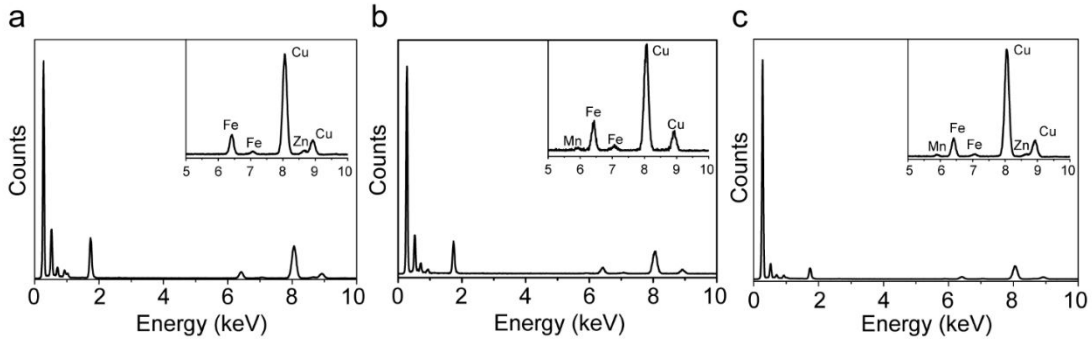

Figure S3. EDX spectra of $Zn_{0.4}F$ (a), γ-Fe_2O_3@$Mn_{0.4}F$ (b), and $Zn_{0.4}F$@$Zn_{0.4}Mn_{0.2}F$ (c).

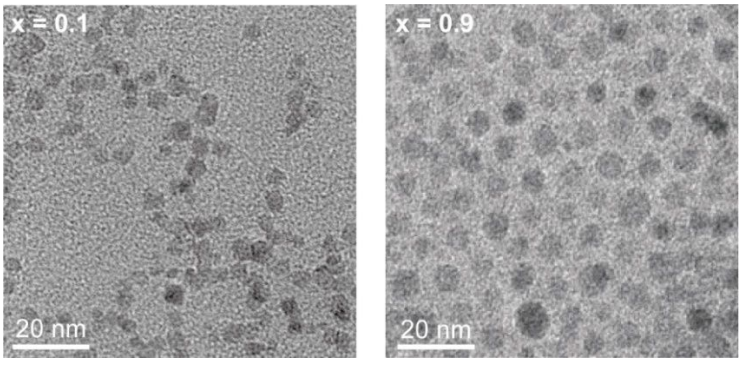

Figure S4. TEM images of $Zn_{0.1}F$ and $Zn_{0.9}F$.

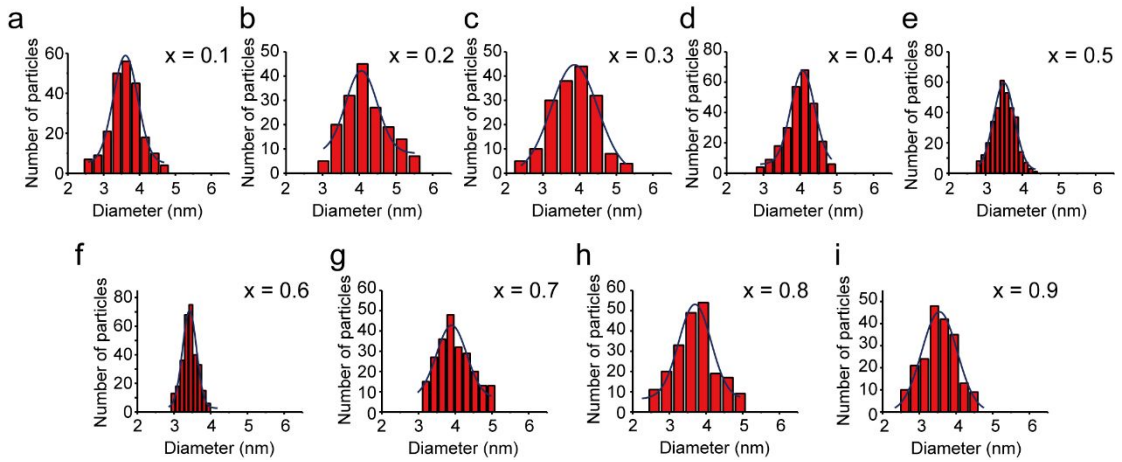

Figure S5. The diameter histograms of the as-synthesized ultrasmall Zn_xF nanoparticles measured from the TEM images.

Table S3. The size, magnetization, and MR relaxivities of the Zn_xF nanoparticles at 300 K

Samples	Size (nm)	Ms (emu/g)	r_1 ($mM^{-1}s^{-1}$)	r_2 ($mM^{-1}s^{-1}$)	r_2/r_1
$Zn_{0.1}F$	3.7±0.5	33.00	3.85	34.18	8.88
$Zn_{0.2}F$	4.1±0.5	37.77	4.28	51.55	12.04
$Zn_{0.3}F$	3.8±0.5	44.29	10.05	69.34	6.9
$Zn_{0.4}F$	4.1±0.4	51.13	13.77	77.32	5.61
$Zn_{0.5}F$	3.5±0.3	50.43	11.49	77.26	6.73
$Zn_{0.6}F$	3.4±0.2	48.62	10.24	72.37	7.07
$Zn_{0.7}F$	3.9±0.5	39.80	7.18	55.74	7.76
$Zn_{0.8}F$	3.7±0.4	30.80	3.18	33.92	10.67
$Zn_{0.9}F$	3.6±0.3	11.20	1.3	18.33	14.1

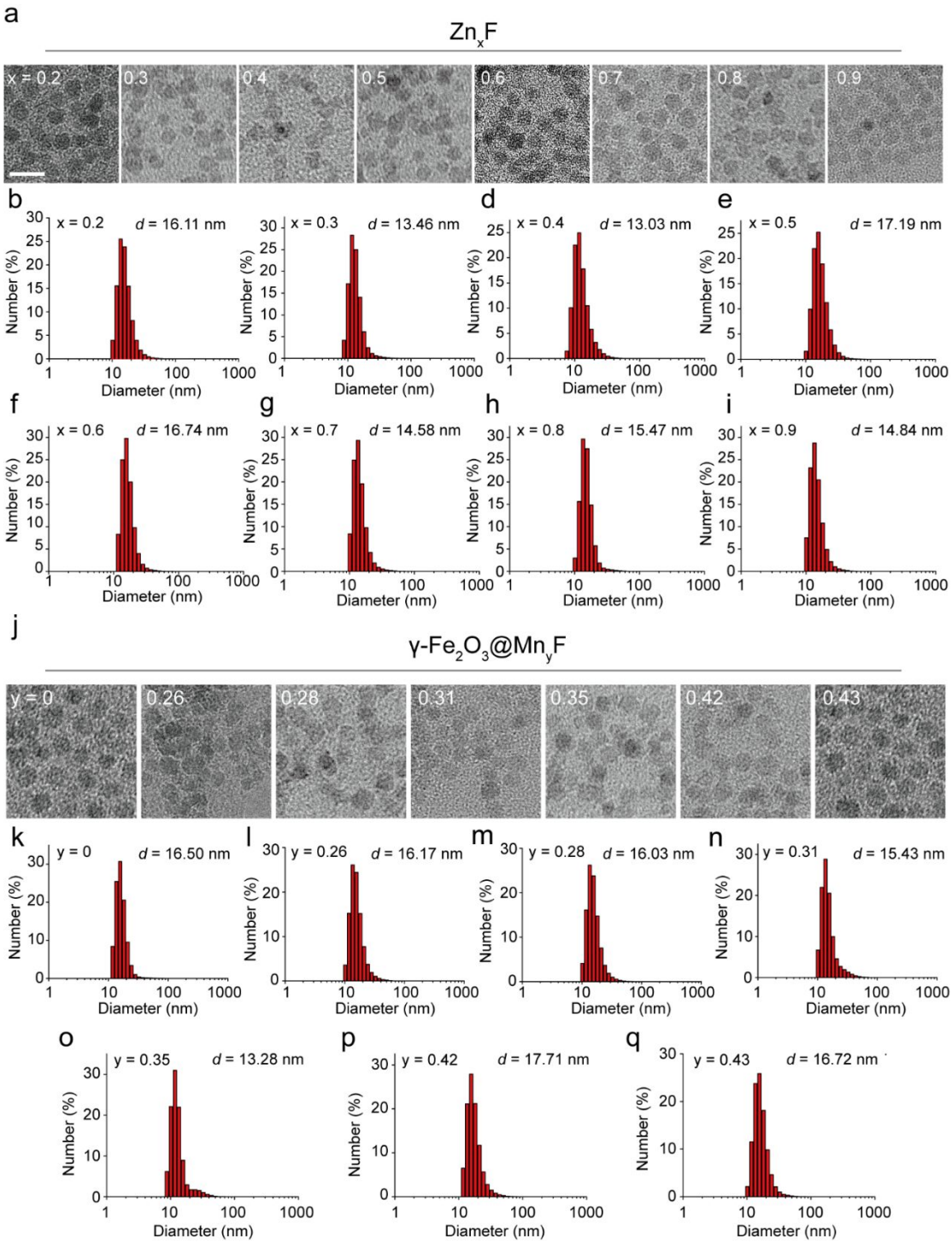

Figure S6. Characterization of water-soluble UFNPs:TEM images of Zn_xF (a) and γ-Fe_2O_3@Mn_yF (j). Hydrodynamic size of Zn_xF (b-i) and γ-Fe_2O_3@Mn_yF (k-q). The as-transferred UFNPs were fairly monodisperse without aggregation and nearly no discernable change after the ligand exchange process. The hydrodynamic diameter of the ligand-exchanged UFNPs was around 15 nm, which confirmed no aggregation of the nanocrystals.

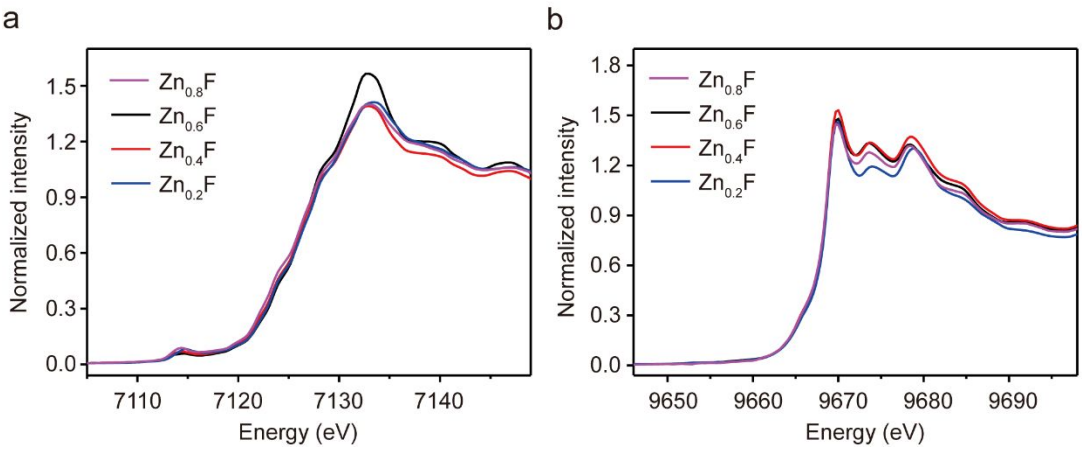

Figure S7. (a) Fe, and (b) Zn K-edge XANES spectra of Zn_xF nanoparticles.

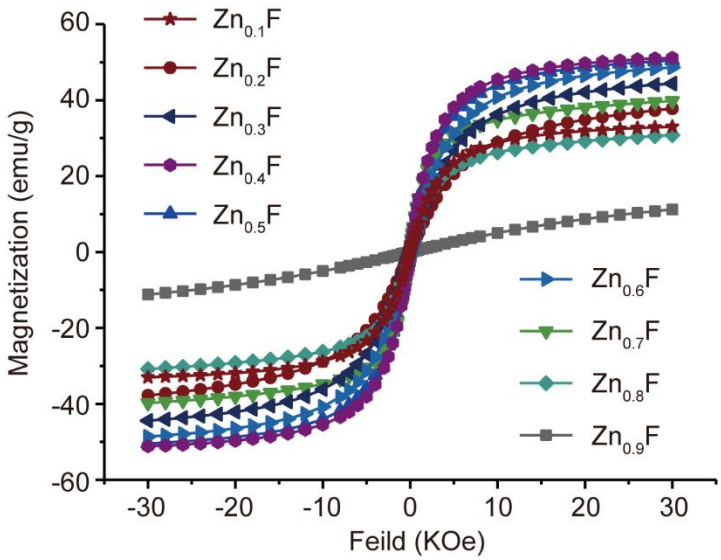

Figure S8. Hysteresis loops of Zn_xF nanoparticles at 300K.

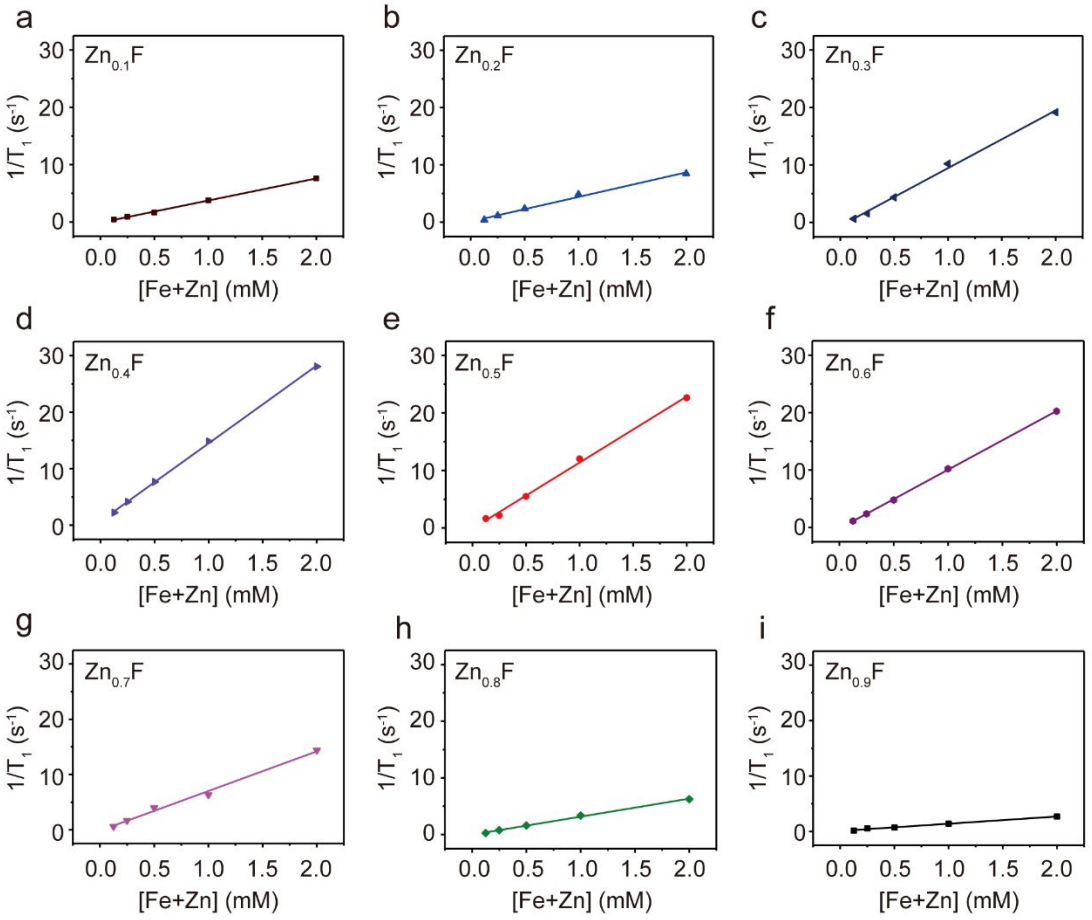

Figure S9. Plots of $1/T_1$ over [Fe+Zn] concentrations of Zn_xF nanoparticles.

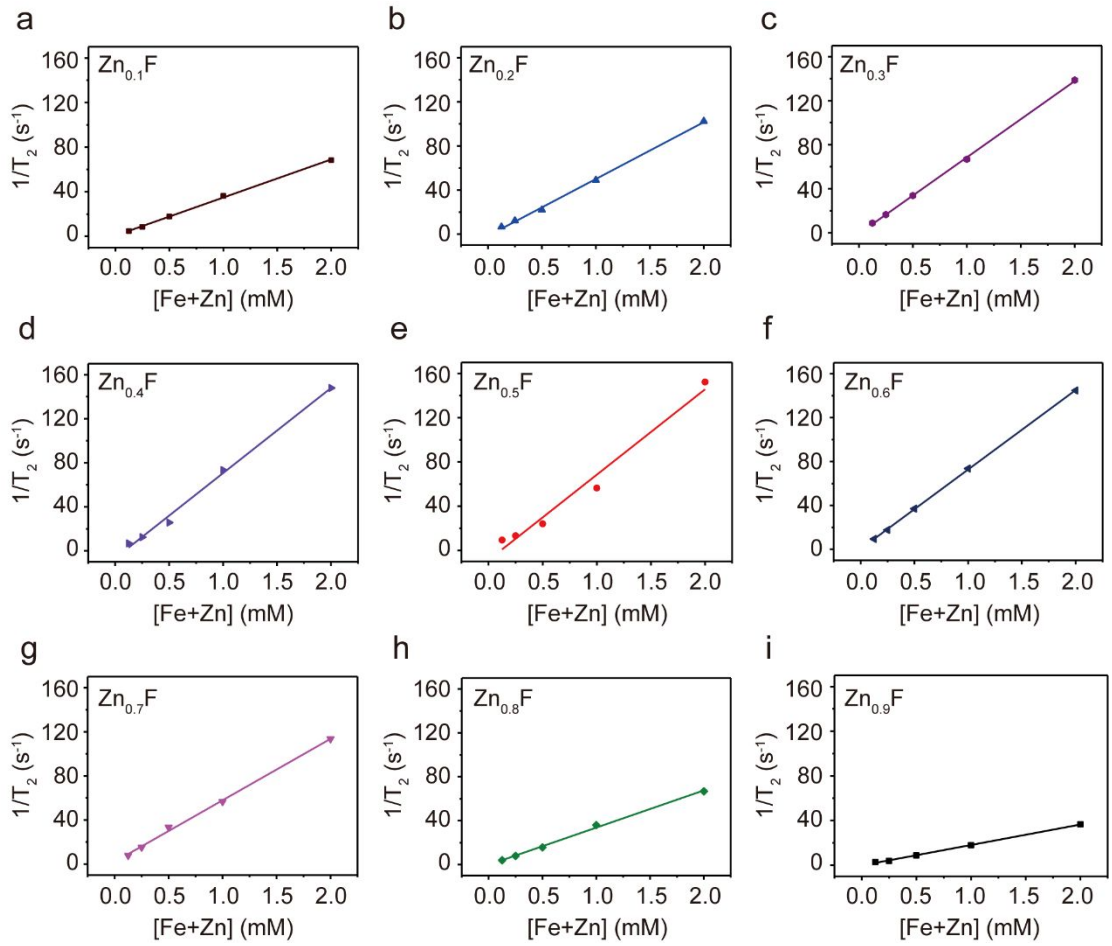

Figure S10. Plots of $1/T_2$ over [Fe+Zn] concentrations of Zn_xF nanoparticles.

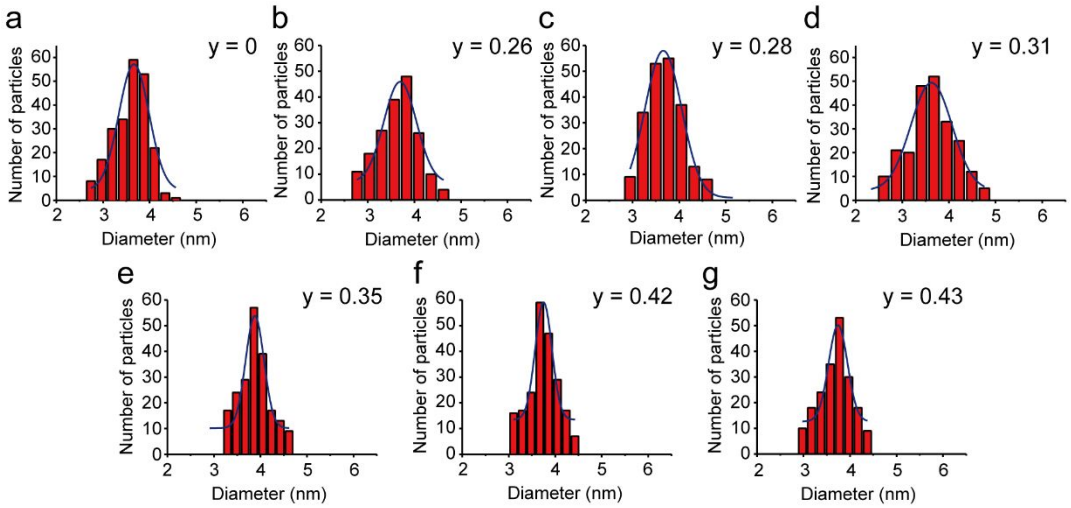

Figure S11. The diameter histograms of γ-Fe_2O_3@Mn_yF nanoparticles.

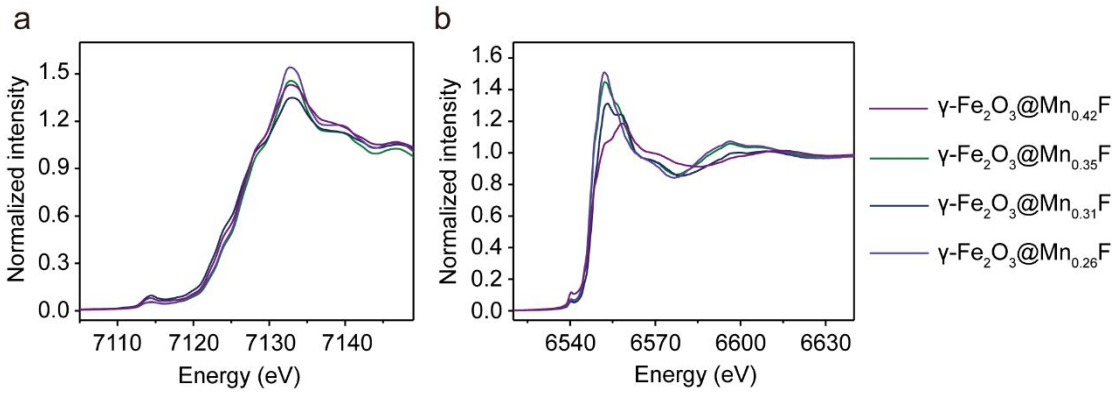

Figure S12. (a) Fe and (b) Mn K-edge XANES spectra of γ-Fe_2O_3@Mn_yF nanoparticles.

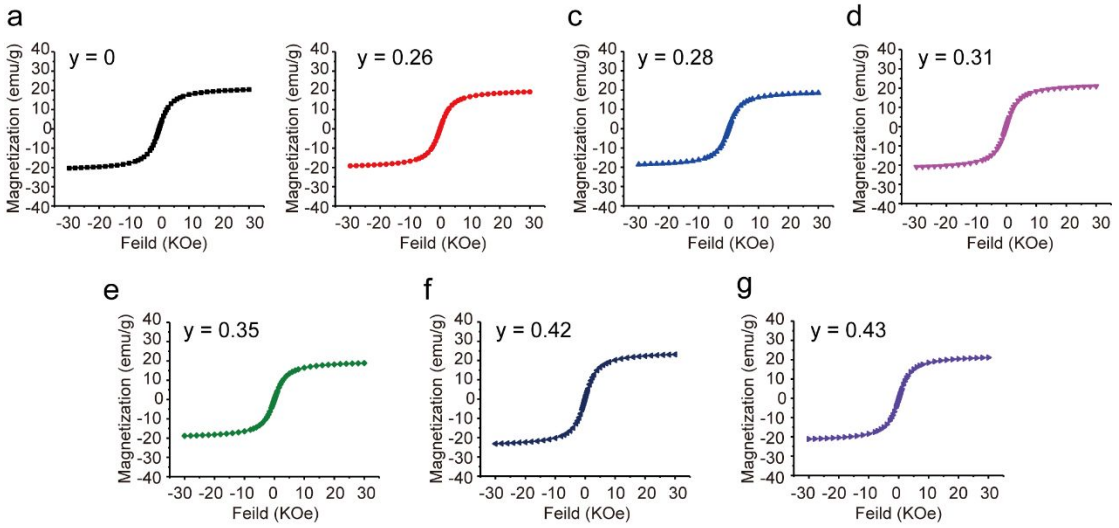

Figure S13. Magnetic hysteresis loops of γ-Fe_2O_3@Mn_yF at 300K.

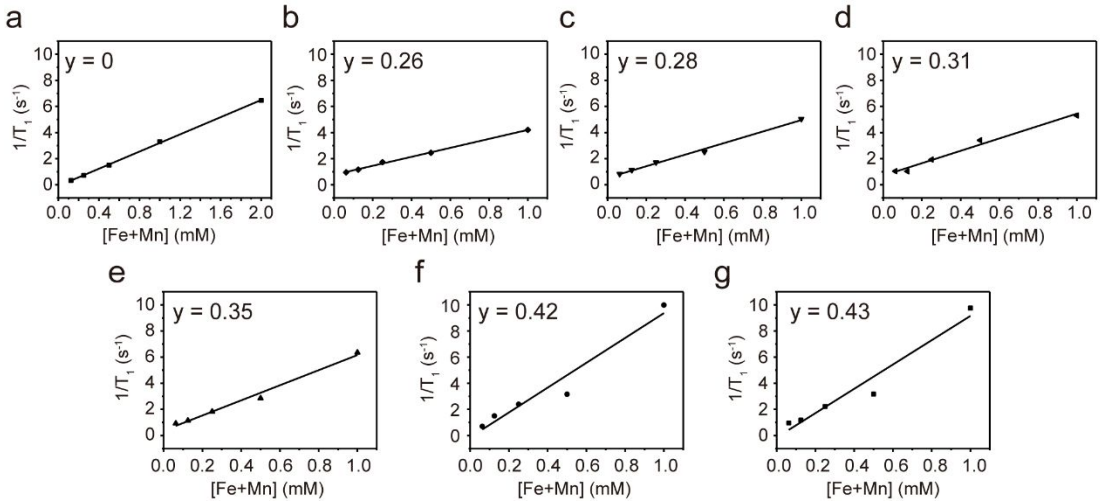

Figure S14. Plots of $1/T_1$ over [Fe+Mn] concentrations of γ-Fe_2O_3@Mn_yF.

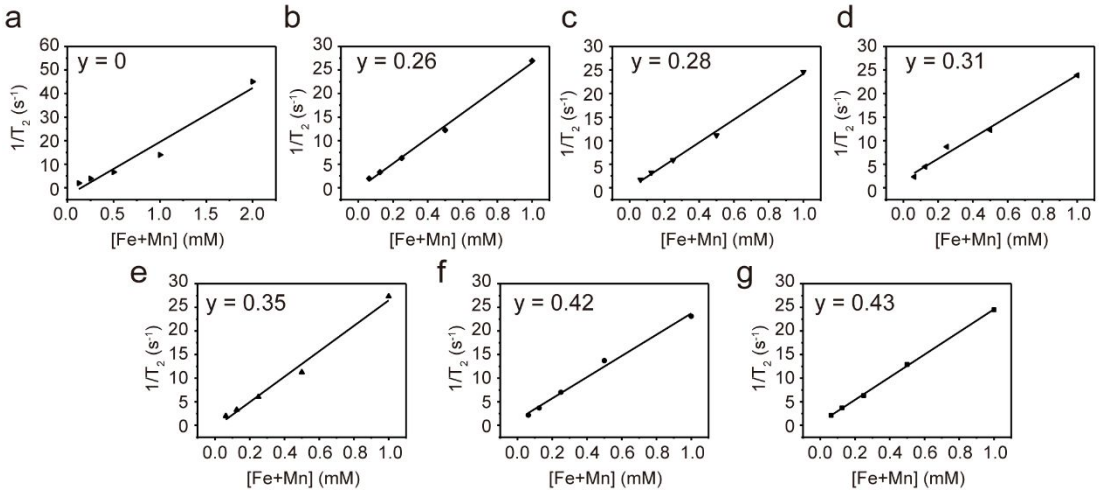

Figure S15. Plots of $1/T_2$ over [Fe+Mn] concentrations of γ-Fe_2O_3@Mn_yF.

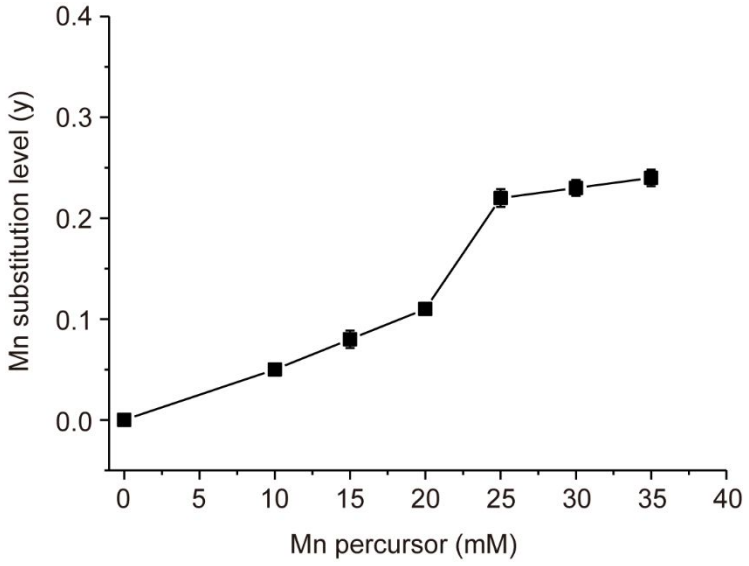

Figure S16. Mn substitution level (y) of $Zn_{0.4}F$@$Zn_{0.4}Mn_yF$ as a function of the concentration of Mn precursor.

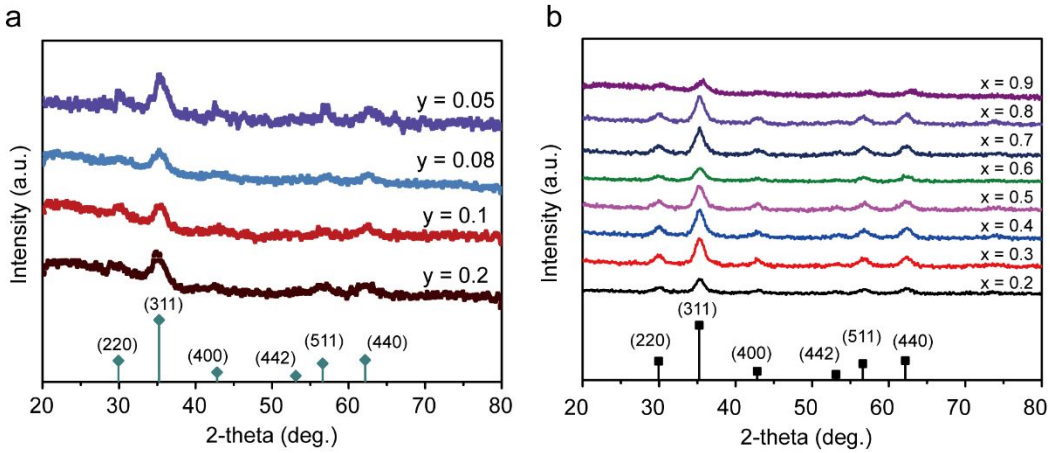

Figure S17. XRD pattens of (a) $Zn_{0.4}F@Zn_{0.4}Mn_yF$ (y = 0.05-0.2) and (b) $Zn_xF@Zn_xMn_{0.2}F$ (x = 0.2-0.9).

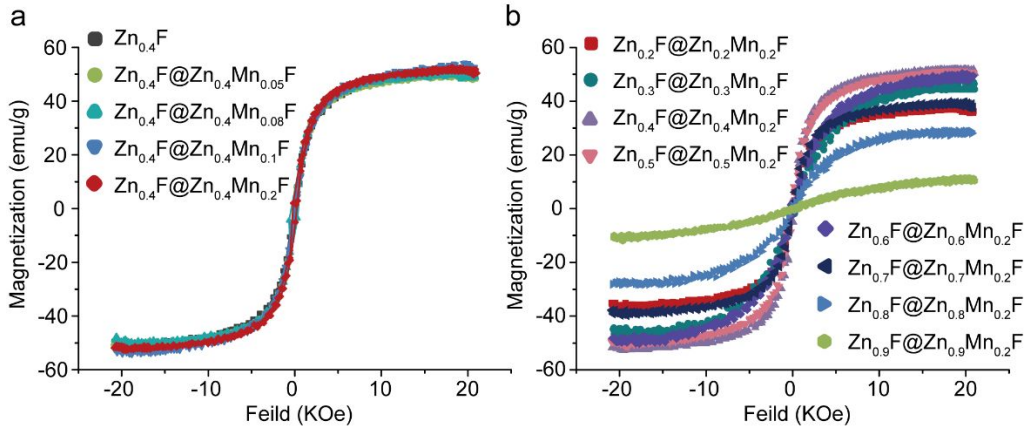

Figure S18. The hysteresis loop of (a) $Zn_{0.4}F@Zn_{0.4}MnyF$ (y = 0-0.2) and (b) $Zn_xF@Zn_xMn_{0.2}F$ (x = 0.2-0.9).

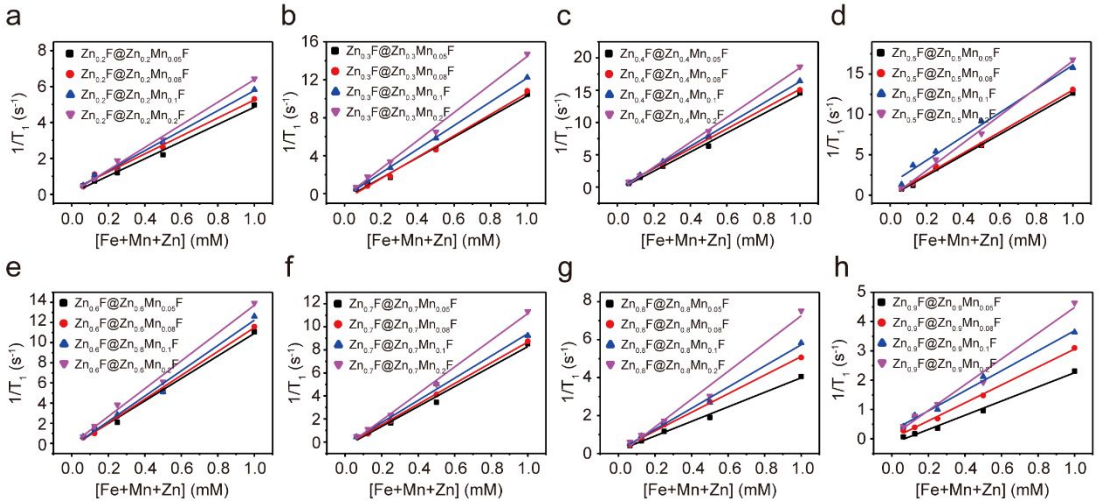

Figure S19. Plots of $1/T_1$ over [Fe+Mn+Zn] concentrations of $Zn_xF@Zn_xMn_yF$ nanoparticles.

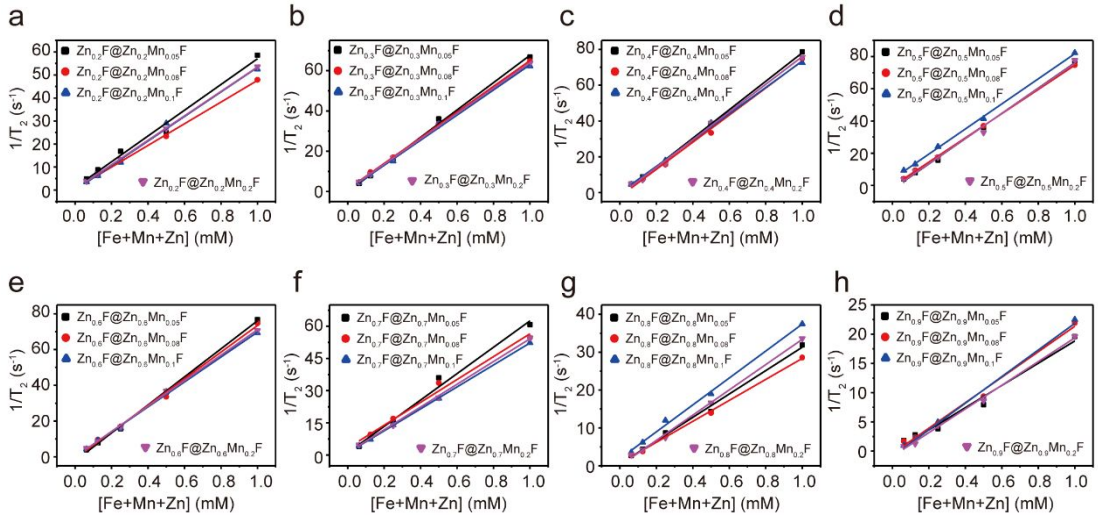

Figure S20. Plots of $1/T_2$ over [Fe+Mn+Zn] concentrations of $Zn_xF@Zn_xMn_yF$ nanoparticles.

Table S4. MR relaxivities of $Zn_xF@Zn_xMn_yF$ nanoparticles.

Samples	r_1 ($mM^{-1}s^{-1}$)	r_2 ($mM^{-1}s^{-1}$)	r_2/r_1
$Zn_{0.2}F@Zn_{0.2}Mn_{0.05}F$	4.79	55.92	11.67
$Zn_{0.2}F@Zn_{0.2}Mn_{0.08}F$	5.01	47.05	9.39
$Zn_{0.2}F@Zn_{0.2}Mn_{0.1}F$	5.59	53.29	9.53
$Zn_{0.2}F@Zn_{0.2}Mn_{0.2}F$	6.30	53.02	8.42
$Zn_{0.3}F@Zn_{0.3}Mn_{0.05}F$	10.81	67.84	6.28
$Zn_{0.3}F@Zn_{0.3}Mn_{0.08}F$	11.25	63.85	5.68
$Zn_{0.3}F@Zn_{0.3}Mn_{0.1}F$	12.49	62.4	5.00
$Zn_{0.3}F@Zn_{0.3}Mn_{0.1}F$	14.76	62.95	4.26
$Zn_{0.4}F@Zn_{0.4}Mn_{0.05}F$	14.82	79.51	5.37
$Zn_{0.4}F@Zn_{0.4}Mn_{0.08}F$	15.35	75.72	4.93
$Zn_{0.4}F@Zn_{0.4}Mn_{0.1}F$	16.67	73.42	4.40
$Zn_{0.4}F@Zn_{0.4}Mn_{0.2}F$	20.22	77.31	3.82
$Zn_{0.5}F@Zn_{0.5}Mn_{0.05}F$	12.75	78.38	6.15
$Zn_{0.5}F@Zn_{0.5}Mn_{0.08}F$	13.04	75.14	5.76
$Zn_{0.5}F@Zn_{0.5}Mn_{0.1}F$	14.72	77.84	5.29
$Zn_{0.5}F@Zn_{0.5}Mn_{0.2}F$	16.94	77.97	4.60
$Zn_{0.6}F@Zn_{0.6}Mn_{0.05}F$	11.17	78.38	7.02
$Zn_{0.6}F@Zn_{0.6}Mn_{0.08}F$	11.84	74.38	6.28
$Zn_{0.6}F@Zn_{0.6}Mn_{0.1}F$	12.56	69.67	5.55
$Zn_{0.6}F@Zn_{0.6}Mn_{0.2}F$	13.80	71.1	5.15
$Zn_{0.7}F@Zn_{0.7}Mn_{0.05}F$	8.66	61.52	7.10
$Zn_{0.7}F@Zn_{0.7}Mn_{0.08}F$	8.98	53.31	5.94

$Zn_{0.7}F@Zn_{0.7}Mn_{0.1}F$	9.64	51.2	5.31
$Zn_{0.7}F@Zn_{0.7}Mn_{0.2}F$	11.58	53.01	4.58
$Zn_{0.8}F@Zn_{0.8}Mn_{0.05}F$	3.83	30.86	8.06
$Zn_{0.8}F@Zn_{0.8}Mn_{0.08}F$	4.90	27.68	5.65
$Zn_{0.8}F@Zn_{0.8}Mn_{0.1}F$	5.58	35.55	6.37
$Zn_{0.8}F@Zn_{0.8}Mn_{0.2}F$	7.32	33.35	4.56
$Zn_{0.9}F@Zn_{0.9}Mn_{0.05}F$	2.42	19.00	7.85
$Zn_{0.9}F@Zn_{0.9}Mn_{0.08}F$	3.06	21.76	7.11
$Zn_{0.9}F@Zn_{0.9}Mn_{0.1}F$	3.41	22.73	6.67
$Zn_{0.9}F@Zn_{0.9}Mn_{0.2}F$	4.39	20.23	4.61

Table S5. The gray-level values of the T_1-weighted images of $Zn_xF@Zn_xMn_yF$.

x/y	0.2	0.3	0.4	0.5	0.6	0.7	0.8	0.9
0.05	86.19	206.149	229.351	207.079	190.794	174.212	66.037	49.566
0.08	128.417	211.639	231.856	215.042	204.594	193.051	116.013	57.399
0.1	142.05	211.974	238.749	230.351	225.047	193.768	140.17	64.628
0.2	152.051	236.548	246.672	230.497	227.131	208.042	169.05	84.503

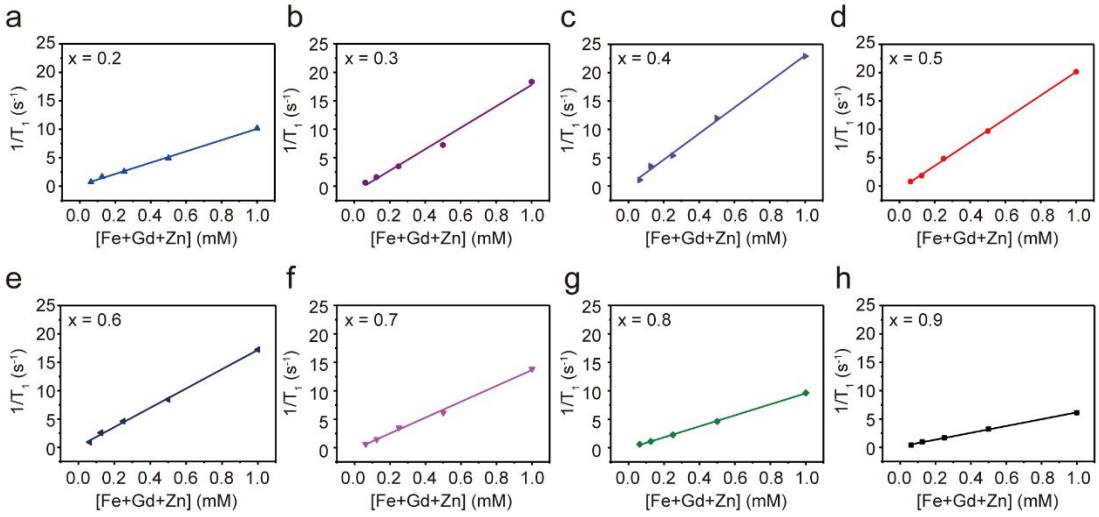

Figure S21. Plots of $1/T_1$ over [Fe+Gd+Zn] concentrations of $Zn_xF@Zn_xGd_{0.2}F$ nanoparticles.

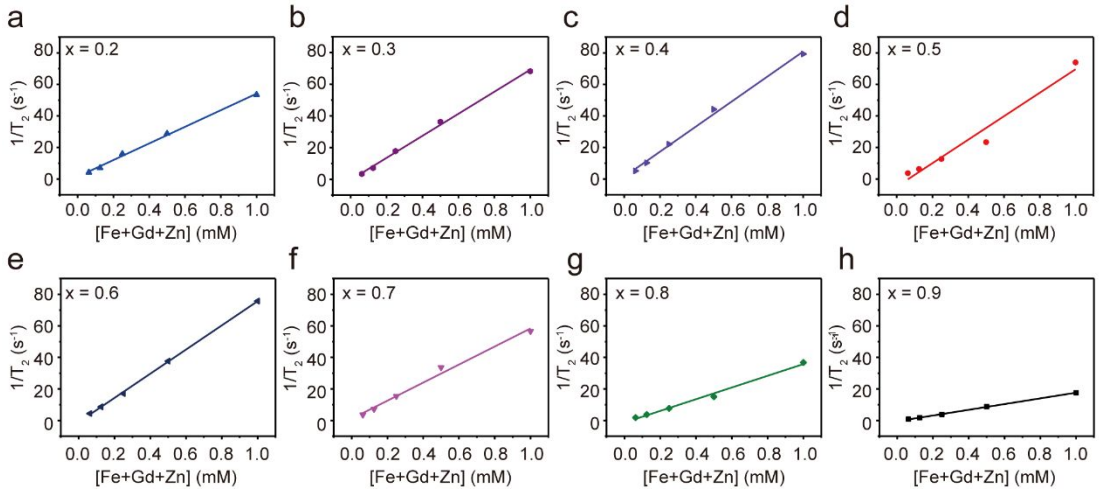

Figure S22. Plots of $1/T_2$ over [Fe+Gd+Zn] concentrations of $Zn_xF@Zn_xGd_{0.2}F$ nanoparticles.

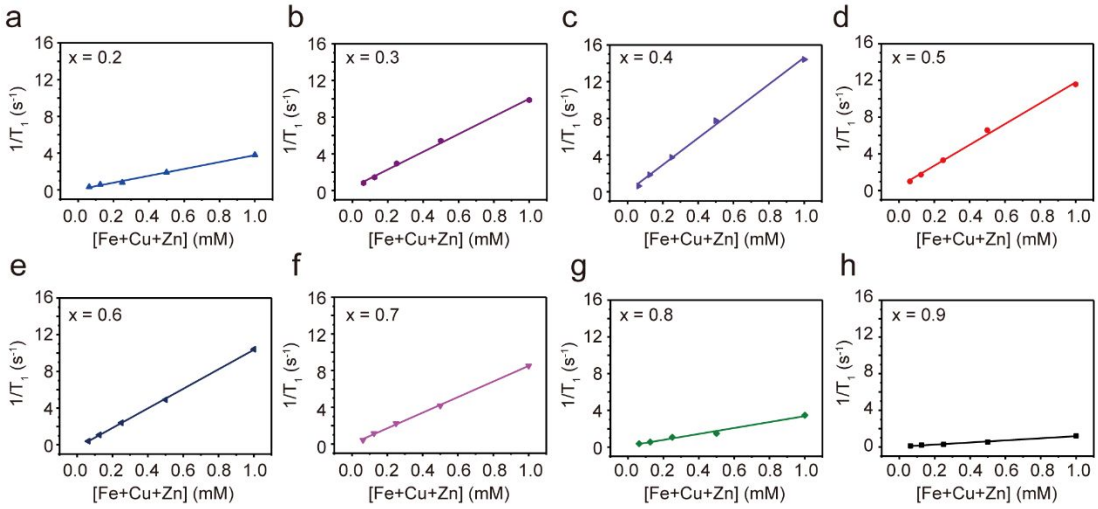

Figure S23. Plots of $1/T_1$ over [Fe+Cu+Zn] concentrations of $Zn_xF@Zn_xCu_{0.2}F$ nanoparticles.

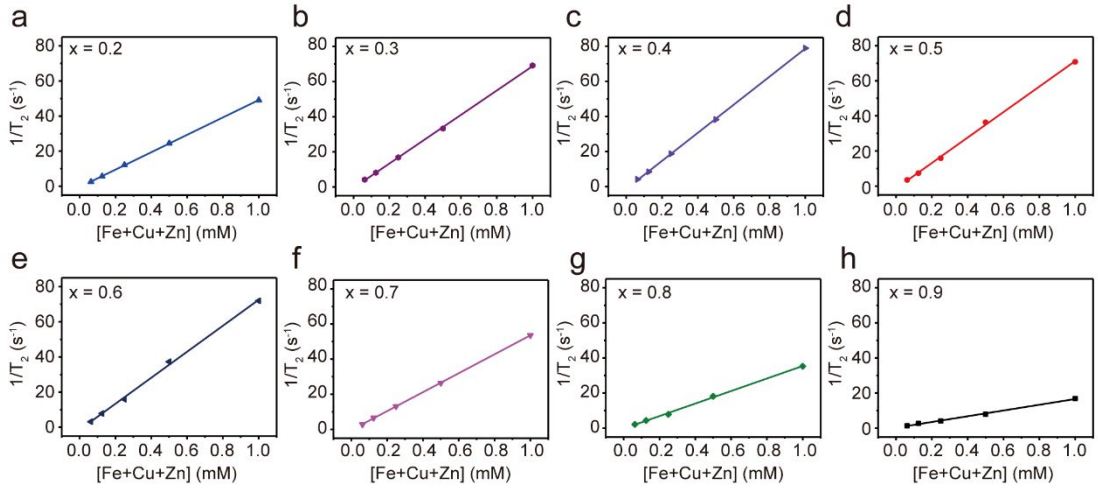

Figure S24. Plots of $1/T_2$ over [Fe+Cu+Zn] concentrations of $Zn_xF@Zn_xCu_{0.2}F$ nanoparticles.

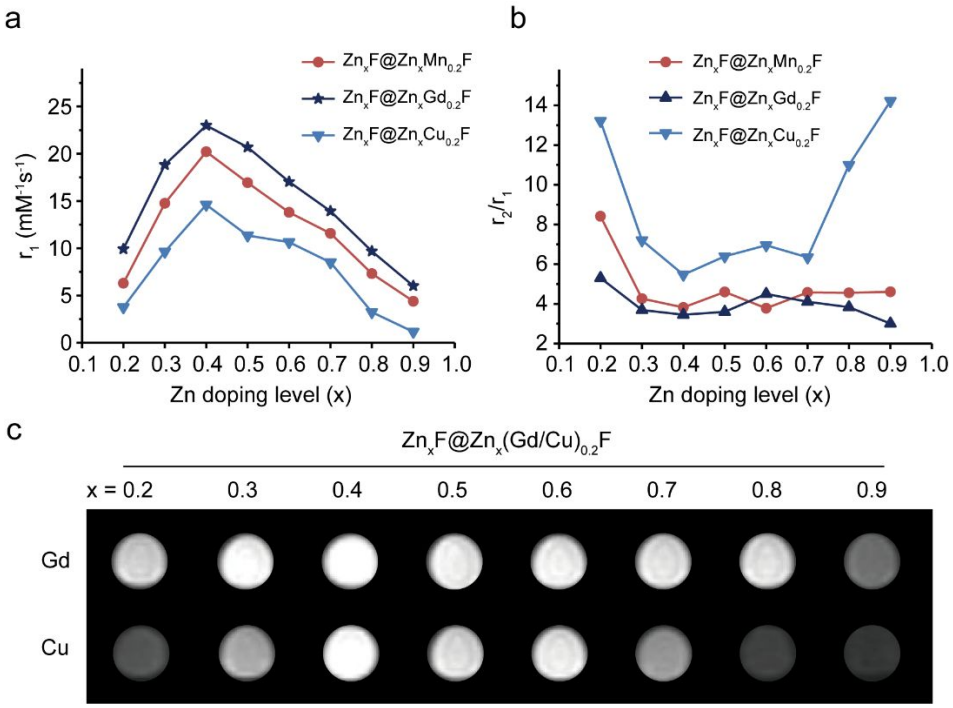

Figure S25. The r_1 relaxivities (a) and r_2/r_1 ratios (b) of $Zn_xF@Zn_xGd_{0.2}F$ and $Zn_xF@Zn_xCu_{0.2}F$ nanoparticles. (c) T_1 weighted images of $Zn_xF@Zn_xGd_{0.2}F$ and $Zn_xF@Zn_xCu_{0.2}F$ nanoparticles ($C_{[Zn+Mn+Fe]}$ = 0.5 mM).

Table S6. MR relaxivities of $Zn_xF@Zn_xGd_{0.2}F$ nanoparticles at 3T

Samples	r_1 ($mM^{-1}s^{-1}$)	r_2 ($mM^{-1}s^{-1}$)	r_2/r_1
$Zn_{0.2}F@Zn_{0.2}Gd_{0.2}F$	9.92	52.62	5.30
$Zn_{0.3}F@Zn_{0.3}Gd_{0.2}F$	18.83	69.56	3.69
$Zn_{0.4}F@Zn_{0.4}Gd_{0.2}F$	22.99	79.40	3.45
$Zn_{0.5}F@Zn_{0.5}Gd_{0.2}F$	20.69	74.45	3.60
$Zn_{0.6}F@Zn_{0.6}Gd_{0.2}F$	17.03	76.67	4.50
$Zn_{0.7}F@Zn_{0.7}Gd_{0.2}F$	13.93	57.26	4.11
$Zn_{0.8}F@Zn_{0.8}Gd_{0.2}F$	9.68	37.13	3.84
$Zn_{0.9}F@Zn_{0.9}Gd_{0.2}F$	6.02	18.13	3.01

Table S7. MR relaxivities of $Zn_xF@Zn_xCu_{0.2}F$ nanoparticles at 3T

Samples	r_1 ($mM^{-1}s^{-1}$)	r_2 ($mM^{-1}s^{-1}$)	r_2/r_1
$Zn_{0.2}F@Zn_{0.2}Cu_{0.2}F$	3.75	49.56	13.22
$Zn_{0.3}F@Zn_{0.3}Cu_{0.2}F$	9.63	69.37	7.20
$Zn_{0.4}F@Zn_{0.4}Cu_{0.2}F$	14.61	79.93	5.47
$Zn_{0.5}F@Zn_{0.5}Cu_{0.2}F$	11.35	72.59	6.40
$Zn_{0.6}F@Zn_{0.6}Cu_{0.2}F$	10.64	73.97	6.95
$Zn_{0.7}F@Zn_{0.7}Cu_{0.2}F$	8.50	53.91	6.34
$Zn_{0.8}F@Zn_{0.8}Cu_{0.2}F$	3.24	35.63	11.00
$Zn_{0.9}F@Zn_{0.9}Cu_{0.2}F$	1.15	16.35	14.22

Table S8. Comparsion of the relaxivitives reported for ultrasmall ferrite nanoparticles

NPs	Size (nm)	r_1 ($mM^{-1}s^{-1}$)	r_2 ($mM^{-1}s^{-1}$)	r_2/r_1	H (T)	Ref
$Zn_{0.4}F@Zn_{0.4}Mn_{0.2}F$	3.8	20.22	77.31	3.82	3.0	This work
$CoFe_2O_4$	2.4	0.746	48.7	48.7	9.4	[6]
		2.11	7.8	3.7	3.0	
γ-Fe_2O_3	3	5.2	10.5	2.0	1.5	[7]
		1.5	17	11	7.0	
γ-Fe_2O_3	2	3.91	5.84	1.49	3.0	[8]
		2.32 ± 0.15	24.4 ± 3.6	10.5 ± 1.3	7.0	
γ-Fe_2O_3	3.6	8.80	22.7	2.6	1.5	[9]
		12.66±1.55	23.5±3.2	1.9±0.1	0.5	
$MnFe_2O_4$	3	8.23	21.97	2.67	3.0	[1]
Fe_3O_4	3.6	4.20	48.8	11.6	3.0	[5]
GdIO	4.8	7.85	41.14	5.24	7.0	[10]
Fe_3O_4	2.2	6.15	28.62	4.65	1.4	[11]
Fe_3O_4	1.9	1.415	2.87	2.03	7.0	[12]
$MnFe_2O_4$	2.2	4.8	17.5	3.65	3.0	[13]
Fe_3O_4	4	5.991	15.534	2.59		
$ZnFe_2O_4$	4	7.928	14.642	1.85	0.5	[14]
$NiFe_2O_4$	5	6.850	12.921	1.89		

Fe_3O_4	3.3	8.3	35.1	4.2	4.7	[15]
Fe_3O_4	5.4	19.7	39.5	2	1.5	[16]
γ-Fe_2O_3	2.2	4.78	17.5	3.67	3.0	[17]
	3	4.77	29.2	6.12		
Fe_3O_4	4	7.3	17.5	2.4	1.41	[18]
γ-Fe_2O_3	1.7	4.46	15.01	3.4	1.5	[19]

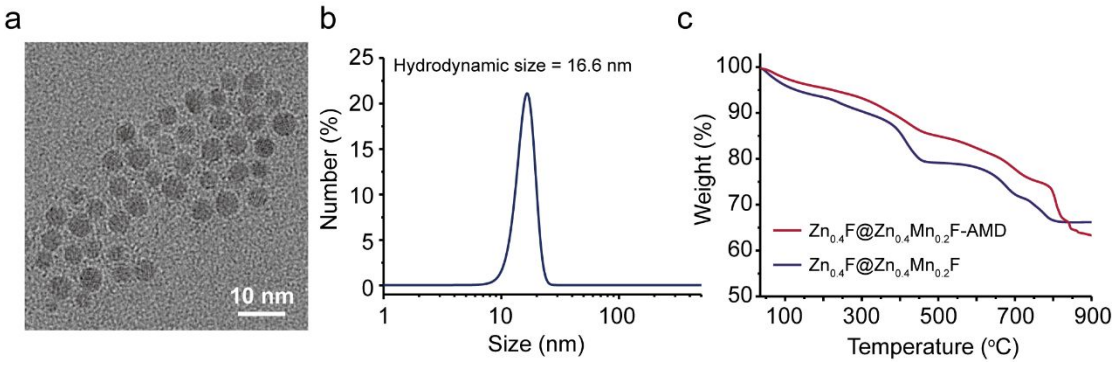

Figure S26. (a) TEM images of $Zn_{0.4}F@Zn_{0.4}Mn_{0.2}F$-AMD. (b) Hydrodynamic size of $Zn_{0.4}F@Zn_{0.4}Mn_{0.2}F$-AMD. (c) Thermogravimetric analysis (TGA) curves of $Zn_{0.4}F@Zn_{0.4}Mn_{0.2}F$ and $Zn_{0.4}F@Zn_{0.4}Mn_{0.2}F$-AMD. The amount of AMD3100 in $Zn_{0.4}F@Zn_{0.4}Mn_{0.2}F$-AMD is estimated to be about 4.6%.

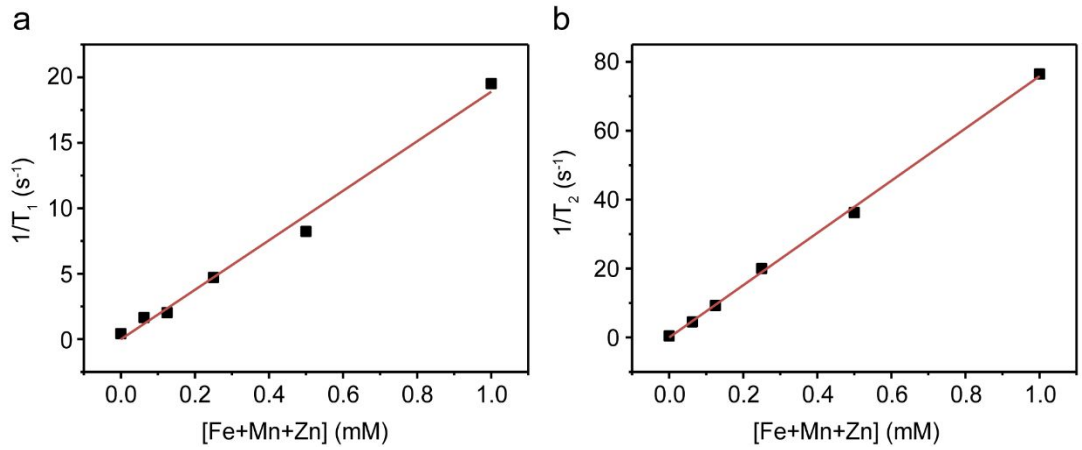

Figure S27. Plot of r_1 value (a) and r_2 value (b) of $Zn_{0.4}F@Zn_{0.4}Mn_{0.2}F$-AMD.

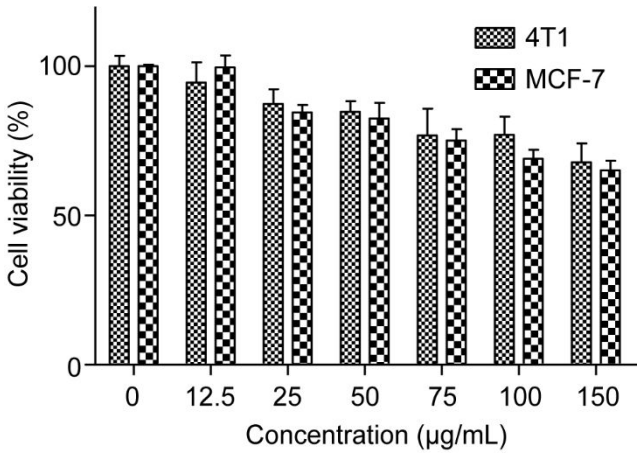

Figure S28. Viabilities of the cells treated with $Zn_{0.4}F@Zn_{0.4}Mn_{0.2}F$-AMD. *In vitro* cytotoxicity assays reveal insignificant toxicity of $Zn_{0.4}F@Zn_{0.4}Mn_{0.2}F$-AMD at a Fe concentration of less than 50 μg/mL.

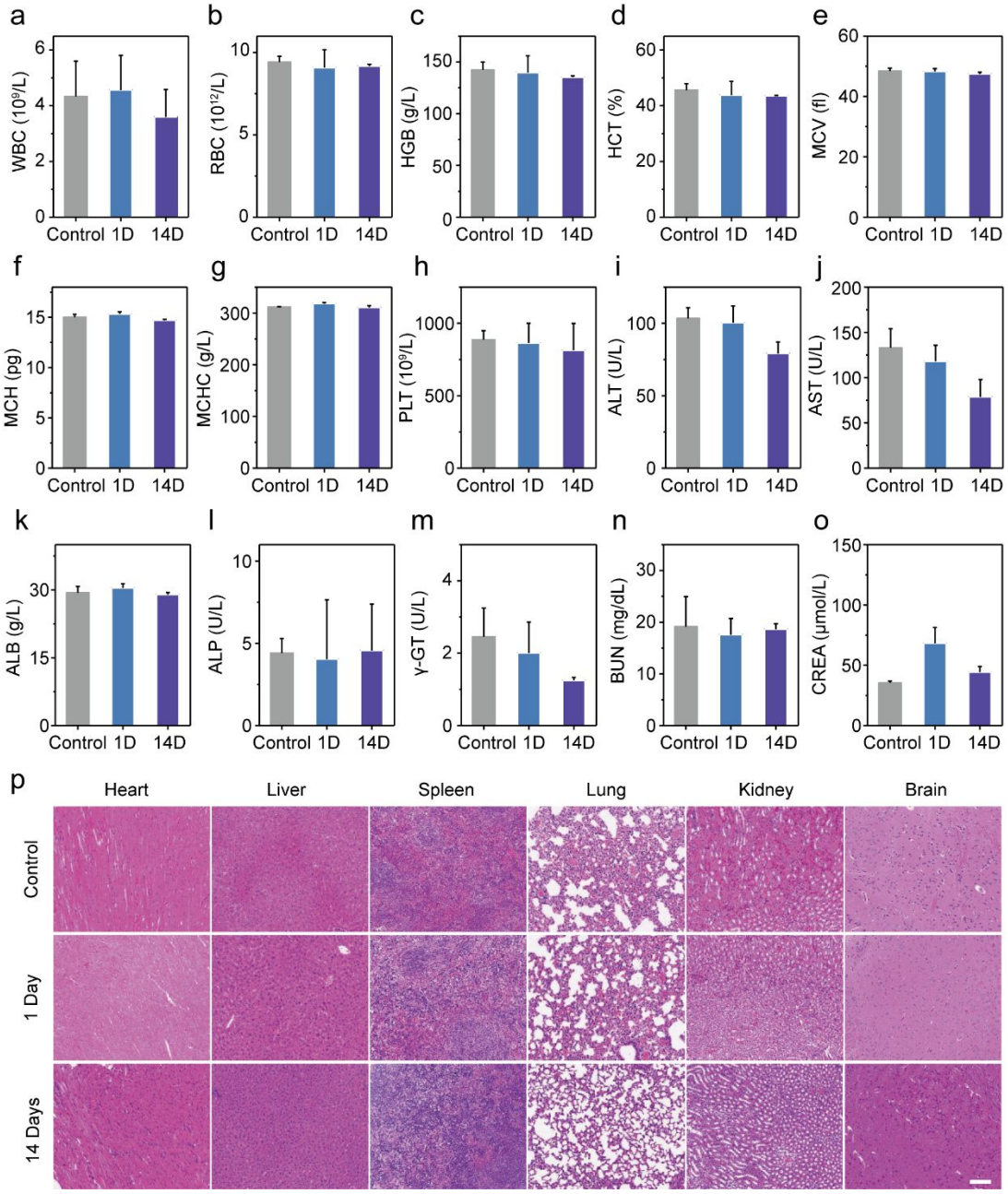

Figure S29. *In vivo* toxicology assessment of $Zn_{0.4}F@Zn_{0.4}Mn_{0.2}F$-AMD. (a-h) Routine blood analysis: (a) white blood cell (WBC), (b) red blood cell (RBC), (c) hemoglobin (HGB), (d) hematocrit (HCT), (e) mean corpuscular volume (MCV), (f) mean corpuscular hemoglobin (MCH), (g) mean corpuscular hemoglobin concentration (MCHC) and (h) platelets (PLT); (i-o) Blood biochemistry analysis: (i) alanine transferase (ALT), (j) aspartate transferase (AST), (k) albumin (ALB), (l) alkaline

phosphatase (ALP), (m) γ-glutamyltransferase (γ-GT), (n) blood urea nitrogen (BUN) and (o) creatinine (CREA); (p) H&E stained images of tissues (heart, liver, spleen, lung, kidney, and brain) of the mice harvested from the control group and treated groups at 1 and 14 days after intravenous injection of $Zn_{0.4}F@Zn_{0.4}Mn_{0.2}F$-AMD. Scale bar = 100 μm. *In vivo* toxicology analysis show that all the blood routine and blood biochemistry markers are within the normal ranges, which suggests good hemocompatibility of $Zn_{0.4}F@Zn_{0.4}Mn_{0.2}F$-AMD. H&E staining examination shows that the $Zn_{0.4}F@Zn_{0.4}Mn_{0.2}F$-AMD treated mice exhibit no visible inflammation or damage.

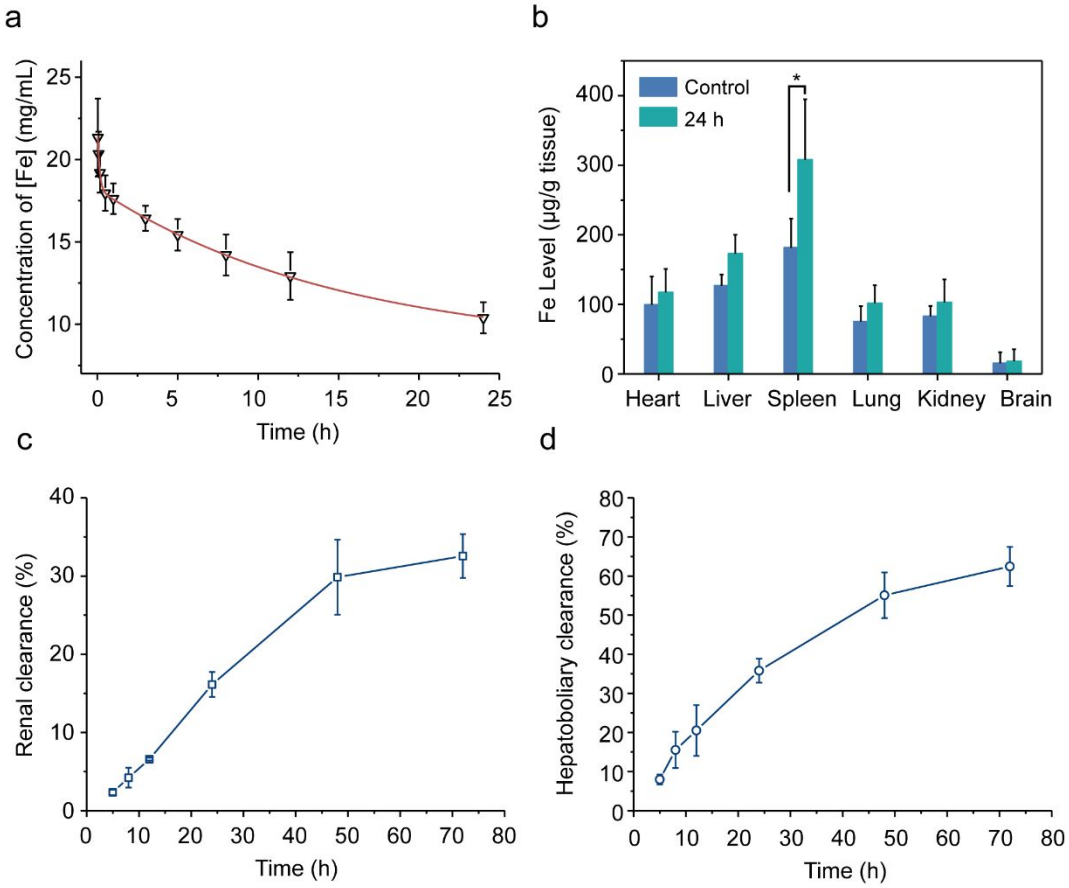

Figure S30. (a) Blood pharmacokinetics of $Zn_{0.4}F@Zn_{0.4}Mn_{0.2}F$-AMD. (b) Biodistribution of $Zn_{0.4}F@Zn_{0.4}Mn_{0.2}F$-AMD at 24 h. Percentage of renal (c) and

hepatobiliary (d) excreted quantity with time after i.v. injection of $Zn_{0.4}F@Zn_{0.4}Mn_{0.2}F$-AMD. *P < 0.001. The *In vivo* pharmacokinetic study shows that the distribution half-life ($t_{1/2\alpha}$) and elimination half-life ($t_{1/2\beta}$) of $Zn_{0.4}F@Zn_{0.4}Mn_{0.2}F$-AMD are determined to be 0.13 ± 0.01 h and 15.2 ± 0.5 h, respectively. The biodistribution results indicate that $Zn_{0.4}F@Zn_{0.4}Mn_{0.2}F$-AMD is mainly accumulates in the spleen and liver after 24 h post-injection. To further investigate the clearance pathway, the metal concentrations in the urine and feces were measured. It was found that more than 29.8 ± 4.8% of the $Zn_{0.4}F@Zn_{0.4}Mn_{0.2}F$-AMD are excreted from the body *via* the renal clearance pathway within 48 h and up to 32.6 ± 2.8% after 72 h. About 55.1 ± 5.8% of $Zn_{0.4}F@Zn_{0.4}Mn_{0.2}F$-AMD are cleared through the hepatobiliary system within 48 h, and the excreted quantity increases to 62.5 ± 5.0% after 72 h.

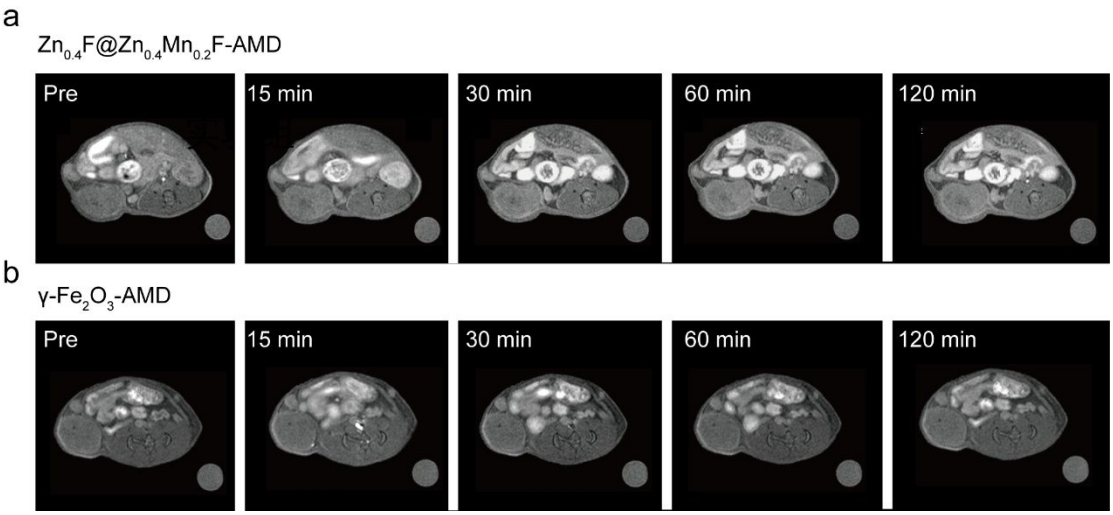

Figure S31. T_1-weighted MR images acquired at the indicated times after intravenous administration of $Zn_{0.4}F@Zn_{0.4}Mn_{0.2}F$-AMD (a) and γ-$Fe_2O_3$-AMD (b).

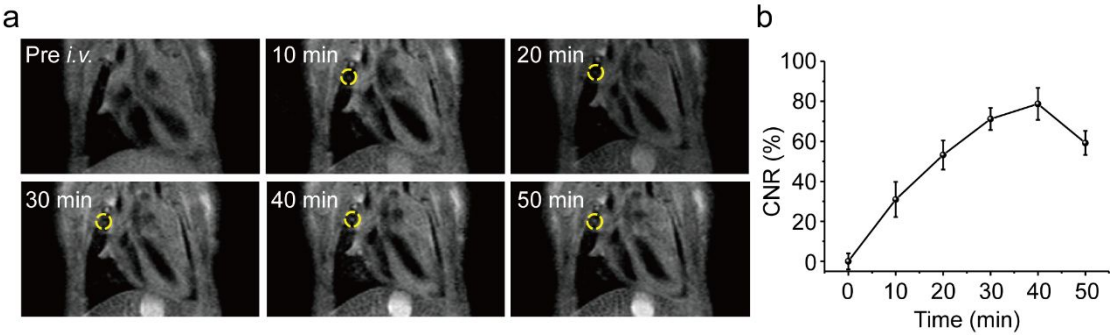

Figure S32. (a) *In vivo* T_1-weighted MR images and (b) CNR of lung metastases after intravenous injection of $Zn_{0.4}F@Zn_{0.4}Mn_{0.2}F$-AMD at 0 min, 10 min, 20 min, 30 min, 40 min, and 50 min post-injection.

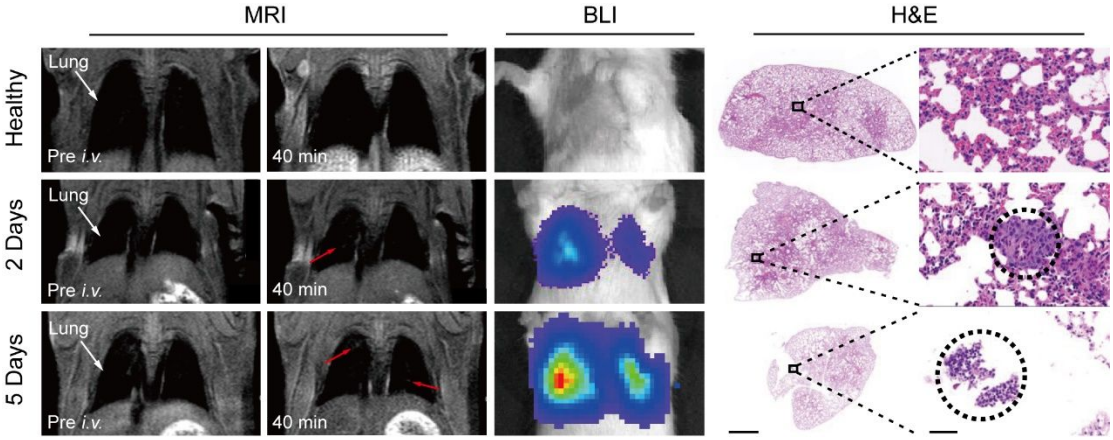

Figure S33. T_1-weighted MR images of metastases in mice subjected to intravenous injection of γ-Fe_2O_3-AMD at 40 min (left: pre-injection, right: post-injection, arrows indicate metastases), and the BLI images and H&E images of the lung (scale bar: left, 1 mm; right, 50 μm).

References

1. Zhang, H.; Li, L.; Liu, X. L.; Jiao, J.; Ng, C. T.; Yi, J. B.; Luo, Y. E.; Bay, B. H.; Zhao, L. Y.; Peng, M. L.; Gu, N.; Fan, H. M., Ultrasmall Ferrite Nanoparticles Synthesized via Dynamic Simultaneous Thermal Decomposition for High-Performance and Multifunctional T_1 Magnetic Resonance Imaging Contrast Agent. *ACS Nano* **2017,** *11* (4), 3614-3631.

2. Liu, Y.; Chen, T.; Wu, C.; Qiu, L.; Hu, R.; Li, J.; Cansiz, S.; Zhang, L.; Cui, C.; Zhu, G.; You, M.; Zhang, T.; Tan, W., Facile surface functionalization of hydrophobic magnetic nanoparticles. *J Am Chem Soc* **2014,** *136* (36), 12552-5.

3. Lauffer, R. E., Paramagnetic Metal Complexes as Water Proton Relaxation Agents for NMR Imaging: Theory and Design. *Chem Rev* **1987,** *87*, 901-927.

4. Caravan, P.; Ellison, J. J.; McMurry, T. J.; Lauffer, R. B., Gadolinium (III) chelates as MRI contrast agents: structure, dynamics, and applications. Chem Rev **1999**, 99 2293-2352.

5. Zeng, J.; Jing, L.; Hou, Y.; Jiao, M.; Qiao, R.; Jia, Q.; Liu, C.; Fang, F.; Lei, H.; Gao, M., Anchoring group effects of surface ligands on magnetic properties of Fe_3O_4 nanoparticles: towards high performance MRI contrast agents. *Adv Mater* **2014**, 26 (17), 2694-2698.

6. Piche, D.; Tavernaro, I.; Fleddermann, J.; Lozano, J. G.; Varambhia, A.; Maguire, M. L.; Koch, M.; Ukai, T.; Hernandez Rodriguez, A. J.; Jones, L.; Dillon, F.; Reyes Molina, I.; Mitzutani, M.; Gonzalez Dalmau, E. R.; Maekawa, T.; Nellist, P. D.; Kraegeloh, A.; Grobert, N., Targeted T_1 Magnetic Resonance Imaging Contrast

Enhancement with Extraordinarily Small $CoFe_2O_4$ Nanoparticles. *ACS Appl Mater Interfaces* **2019,** *11* (7), 6724-6740.

7. Wei, H.; Bruns, O. T.; Kaul, M. G.; Hansen, E. C.; Barch, M.; Wisniowska, A.; Chen, O.; Chen, Y.; Li, N.; Okada, S.; Cordero, J. M.; Heine, M.; Farrar, C. T.; Montana, D. M.; Adam, G.; Ittrich, H.; Jasanoff, A.; Nielsen, P.; Bawendi, M. G., Exceedingly small iron oxide nanoparticles as positive MRI contrast agents. *Proc Natl Acad Sci U S A* **2017,** *114* (9), 2325-2330.

8. Lu, Y.; Xu, Y. J.; Zhang, G. B.; Ling, D.; Wang, M. Q.; Zhou, Y.; Wu, Y. D.; Wu, T.; Hackett, M. J.; Hyo Kim, B.; Chang, H.; Kim, J.; Hu, X. T.; Dong, L.; Lee, N.; Li, F.; He, J. C.; Zhang, L.; Wen, H. Q.; Yang, B.; Hong Choi, S.; Hyeon, T.; Zou, D. H., Iron oxide nanoclusters for T_1 magnetic resonance imaging of non-human primates. *Nat Biomed Eng* **2017,** *1* (8), 637-643.

9. Shen, Z.; Chen, T.; Ma, X.; Ren, W.; Zhou, Z.; Zhu, G.; Zhang, A.; Liu, Y.; Song, J.; Li, Z.; Ruan, H.; Fan, W.; Lin, L.; Munasinghe, J.; Chen, X.; Wu, A., Multifunctional Theranostic Nanoparticles Based on Exceedingly Small Magnetic Iron Oxide Nanoparticles for T_1-Weighted Magnetic Resonance Imaging and Chemotherapy. *ACS Nano* **2017,** *11* (11), 10992-11004.

10. Zhou, Z.; Wang, L.; Chi, X.; Bao, J.; Yang, L.; Zhao, W.; Chen, Z.; Wang, X.; Chen, X.; Gao, J., Engineered Iron-Oxide-Based Nanoparticles as Enhanced T_1 Contrast Agents for Efficient Tumor Imaging. *ACS Nano* **2013,** *7*, 3287-3296.

11. Wang, G.; Zhang, X.; Skallberg, A.; Liu, Y.; Hu, Z.; Mei, X.; Uvdal, K., One-step synthesis of water-dispersible ultra-small Fe_3O_4 nanoparticles as contrast agents for T_1

and T_2 magnetic resonance imaging. *Nanoscale* **2014,** *6* (5), 2953-63.

12. Shen, L. H.; Bao, J. F.; Wang, D.; Wang, Y. X.; Chen, Z. W.; Ren, L.; Zhou, X.; Ke, X. B.; Chen, M.; Yang, A. Q., One-step synthesis of monodisperse, water-soluble ultra-small Fe_3O_4 nanoparticles for potential bio-application. *Nanoscale* **2013,** *5* (5), 2133-41.

13. Li, Z.; Wang, S. X.; Sun, Q.; Zhao, H. L.; Lei, H.; Lan, M. B.; Cheng, Z. X.; Wang, X. L.; Dou, S. X.; Max Lu, G. Q., Ultrasmall manganese ferrite nanoparticles as positive contrast agent for magnetic resonance imaging. *Adv Healthc Mater* **2013,** *2* (7), 958-64.

14. Zeng, L.; Ren, W.; Zheng, J.; Cui, P.; Wu, A., Ultrasmall water-soluble metal-iron oxide nanoparticles as T_1-weighted contrast agents for magnetic resonance imaging. *Phys Chem Chem Phys* **2012,** *14* (8), 2631-6.

15. Li, Z.; Yi, P. W.; Sun, Q.; Lei, H.; Li Zhao, H.; Zhu, Z. H.; Smith, S. C.; Lan, M. B.; Lu, G. Q. M., Ultrasmall Water-Soluble and Biocompatible Magnetic Iron Oxide Nanoparticles as Positive and Negative Dual Contrast Agents. *Advanced Functional Materials* **2012,** *22* (11), 2387-2393.

16. Hu, F.; Jia, Q.; Li, Y.; Gao, M., Facile synthesis of ultrasmall PEGylated iron oxide nanoparticles for dual-contrast T_1- and T_2-weighted magnetic resonance imaging. *Nanotechnology* **2011,** *22* (24), 245604.

17. Kim, B. H.; Lee, N.; Kim, H.; An, K.; Park, Y. I.; Choi, Y.; Shin, K.; Lee, Y.; Kwon, S. G.; Na, H. B.; Park, J. G.; Ahn, T. Y.; Kim, Y. W.; Moon, W. K.; Choi, S. H.; Hyeon, T., Large-scale synthesis of uniform and extremely small-sized iron oxide

nanoparticles for high-resolution T_1 magnetic resonance imaging contrast agents. *J Am Chem Soc* **2011,** *133* (32), 12624-12631.

18. Tromsdorf, U. I.; Bruns, O. T.; Salmen, S. C.; Beisiegel, U.; Weller, H., A Highly Effective, Nontoxic T_1 MR Contrast Agent Based on Ultrasmall PEGylated Iron Oxide Nanoparticles. *Nano Lett* **2009,** *9* (12), 4434-4440.

19. Park, J. Y.; Daksha, P.; Lee, G. H.; Woo, S.; Chang, Y., Highly water-dispersible PEG surface modified ultra small superparamagnetic iron oxide nanoparticles useful for target-specific biomedical applications. *Nanotechnology* **2008,** *19* (36), 365603.